

---

# Knowing When to Quit: Probabilistic Early Exits for Speech Separation Networks

---

Kenny Falkær Olsen<sup>1,2</sup> Mads Østergaard<sup>2</sup> Karl Ulbæk<sup>2</sup> Søren Føns Nielsen<sup>2</sup>  
 Rasmus Malik Høegh Lindrup<sup>2</sup> Bjørn Sand Jensen<sup>1</sup> Morten Mørup<sup>1</sup>

<sup>1</sup>Technical University of Denmark <sup>2</sup>WS Audiology

## Abstract

In recent years, deep learning-based single-channel speech separation has improved considerably, in large part driven by increasingly compute- and parameter-efficient neural network architectures. Most such architectures are, however, designed with a fixed compute and parameter budget, and consequently cannot scale to varying compute demands or resources, which limits their use in embedded and heterogeneous devices such as mobile phones and hearables. To enable such use-cases we design a neural network architecture for speech separation capable of early-exit, and we propose an uncertainty-aware probabilistic framework to jointly model the clean speech signal and error variance which we use to derive probabilistic early-exit conditions in terms of desired signal-to-noise ratios. We evaluate our methods on both speech separation and enhancement tasks, and we show that a single early-exit model can be competitive with state-of-the-art models trained at many compute and parameter budgets. Our framework enables fine-grained dynamic compute-scaling of speech separation networks while achieving state-of-the-art performance and interpretable exit conditions.

## 1 Introduction

The cocktail party problem [53] concerns the separation of a (possibly unknown) number of overlapping speakers, potentially corrupted by environmental noise and reverberation. The task is typically divided into speech separation (separating speakers) and speech enhancement (removing environmental noise), both of which have direct applications in, e.g., telecommunications and hearables.

Single-channel speech separation has become predominantly deep learning-based with the introduction of TasNet [58]. Notable follow-ups include Conv-TasNet [13], which showed that competitive speech separation performance could be achieved at significantly lower computational cost, and SepFormer [9], which showed large performance improvements using a transformer architecture. While the transformer improved modeling performance and training parallelism over prior recurrent and convolutional networks it also ties compute complexity to the length of the attention context window, which can be costly at inference time. For training, these works have primarily relied on the scale-invariant signal-to-noise ratio loss [45] with utterance-level permutation invariant training [39, 40].

Current speech separation architectures typically cannot vary their compute in response to simplifying conditions such as non-overlapping speech, low environmental noise, or silence. Following the terminology in *A Survey on Dynamic Neural Networks* [5], we refer to networks which can vary compute based on either self-estimated difficulty or external conditions as *dynamic*. One approach to dynamic neural networks is *early exit* [67], where the network can make predictions at several depths through the network based on an exit condition. Another is *dynamic routing*, where different

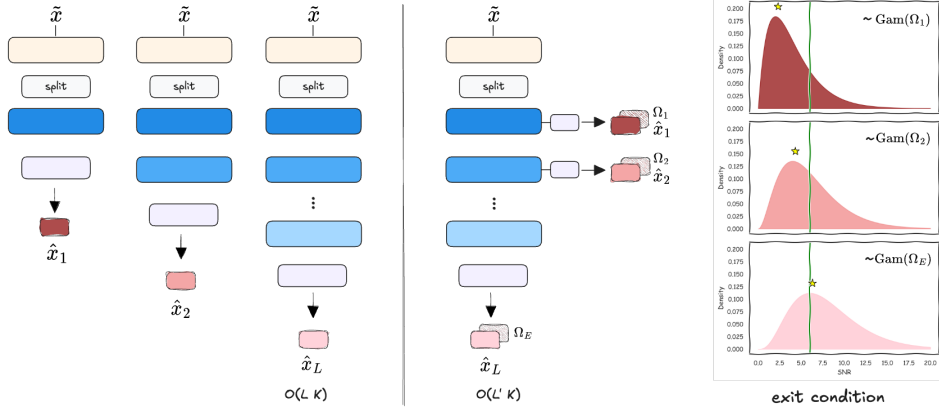


Figure 1: **Knowing when to quit:** Difference between static networks (left) and our probabilistic early-exit method (right). Our model can make predictions at multiple exit-points along with predictive distributions over the SNR improvement (SNRI) with ground truth performance in SNRI marked with a star. The distribution CDF can be thresholded based on a target SNRI level (green vertical line) as an early-exit condition. With a per-block computational requirement,  $K$ , a static  $L$ -layer network will be  $\mathcal{O}(LK)$  but the dynamic network can reduce this to scale with layer at exit,  $L'$ .

subsets of the weights in some layers are used during inference based on a routing condition, such as in mixture-of-experts [1] (MoE) and slimmable networks [51].

Early exit allows direct scaling of both compute and the total number of activated parameters in the network, which allows fine-grained decision making using all information and processing available up to the current exit point. End-to-end training of early-exiting neural networks has also been shown to reduce overfitting and improve gradient propagation during training [67]. In the context of speech separation, a SepReformer [47] trained with additional reconstruction losses reminiscent of early exit improved the final performance of the network.

In this work, we introduce PRobabilistic Early-exit for Speech Separation (PRESS) which leverages early exits to reduce inference costs and improve generalization. Importantly, our approach is probabilistic and naturally assign weights to the different exit conditions by their quantified log-likelihood-based reconstruction quality. At inference time, the probabilistic formulation further enables PRESS to control when to exit computation using the model’s certainty that a desired signal-to-noise ratio (SNR) between the estimated and clean audio signals has been achieved. Specifically, we make the following contributions:

1. We propose a new speech separation architecture designed for early exit and endow the model with uncertainty awareness though a probabilistic model formulation accounting for both the clean speech signal and the variance of the error and its associated uncertainty.
2. We demonstrate that our approach provides a simple and principled framework to balance reconstruction quality and early-exit conditions while circumventing the need for conventional scale- and permutation-invariant training. We further explore that our probabilistic formulation enables predicting the (improvement in) SNR and derive an exit criteria based on the desired SNR level.
3. We validate our approach for both speech separation on the WSJ0-2mix [14] and Libri2Mix [26] datasets, demonstrating the viability of training a single, dynamic neural network with early exits to achieve performance competitive with state-of-the-art static, single-exit models.

## 2 Related Work

**TasNet-family.** TasNet [58] replaced masking in a fixed spectral representation with learnable convolutional encoder and decoder layers. The bulk of parameters and compute of TasNets are in a recurrent neural network (RNN) masker network, which produces masks that are applied to the encoded mixture before decoding to produce single-source estimates. TasNet inspired follow-up work such as computationally efficient variants like the Conv-TasNet [13] and SudoRMRF [57], as well as

the DP-RNN [21] which introduced dual-path processing, decoupling time-mixing operations into chunks. The dual-path structure was also used with transformer-based networks in SepFormer [9], TF-GridNet [60] and MossFormer [32, 33].

**SepReformer** [47] introduces *early splitting*: instead of projecting a shared encoded representation into separate estimated sources late in the network as in TasNet, the projection into separate sources occurs early in the network. Further processing happens independently for each source with only a cross-speaker attention layer enabling information exchange between processing for the sources. SepReformer is constructed as a U-net [65] with a transformer-like stack [8] composed of a convolutional block, a time-mixing attention block, and a cross-speaker attention block, and uses LayerScale [24] to train comparatively deep and slim networks. The network maximizes scale-invariant signal-to-noise ratio (SI-SNR) using utterance-level permutation invariant training (uPIT) with extra loss terms maximizing the SI-SNR of downsampled frequency-domain representations of the estimated sources to encourage early separation of sources.

**Diffusion models, SNR estimation and iterative refinement.** SepIt [48] iteratively refines its estimates and stops processing based on bounding the SNR through mutual information between current estimates and the input mixture—this bound is extended to consider generative models in DiffSep [17]. Diffusion/score-based models like DiffSep can, generally, sample the learned diffusion process with variable compute requirements in a trade-off with quality. For instance, DiffWave [18]—a diffusion-based vocoder also used in separation tasks in Separate and Diffuse [46]—shows faster sampling by reducing needed steps through designing an appropriate variance schedule.

**Slimmable Networks** allow the *width* of the network to be adjusted at inference time to trade-off compute and accuracy have been termed slimmable networks [51, 52, 22]. This can be achieved using switchable batch normalization [51], which essentially, given a predefined set of widths, trains a single network with multiple batch normalization layers, one pr. width. The width specific batch-normalization can be moved to post-training [52], employing knowledge distillation during training while sampling different widths pr. batch. The idea of *dynamic* slimmable networks [22] uses a dynamic gating mechanism that routes the signal to a subset of the next stage in the network to reduce complexity. In the context of speech and audio, Slim-TasNet [50] combines the TasNet architecture for speech separation with width slimming and a given input width size. A dynamic version of this, dynamic slimmable TasNet [23], utilizes a predictive scheme, where each subnetwork predicts how much of the following subnetwork that should be utilized. Similarly, in the context of speech enhancement, dynamic channel pruning [43] is a technique for estimating a mask applied in the channel dimension of convolutional layers, that reduces the runtime computational cost.

**Early Exit.** Various strategies are used to construct exit condition, and to train early-exit models. In classification tasks, such as image classification, the entropy at each exit has been used as an exit condition [11, 16] using pre-softmax logits as a proxy for model uncertainty. In the context of language modeling the Sparse Universal Transformer [54] used a stick-breaking construction to define monotonically increasing halting probabilities which down-weighted intermediate activations in later layers to scale down their influence on the final prediction, which was learned through a single loss. In the context of speech separation, the Euclidean norm difference between successive blocks has been used as an exit condition in a transformer-based architecture [20]. In speech enhancement the PDRE [2] model iteratively applies a deterministic U-net [65] network to the noisy signal and predicts the parameters of a Gaussian mixture model (GMM), to get a distribution over the clean signal at each iteration, and the network is trained to maximize the weighted sum of log-likelihoods of each step’s GMM. However, no stopping criteria or exit-conditions were explored to determine when to stop the enhancement process.

## 3 Method

### 3.1 Probabilistic Speech Separation

We use a Bayesian objective where the target signal  $x \in \mathbb{R}^T$  is modelled by jointly predicting an estimated signal  $\hat{x} \in \mathbb{R}^T$  and a variance  $\sigma^2$  in the prediction, where we assume a Gaussian distribution on the signal error and a conjugate inverse-gamma prior on the variance. Marginalizing

the variance, we obtain the multivariate Student t-distribution likelihood given by:

$$\mathcal{L} = \int \mathcal{N}(\mathbf{x} \mid \hat{\mathbf{x}}, \sigma^2 \mathbf{I}) \text{InvGam}(\sigma^2 \mid \alpha, \beta) d\sigma^2 = \text{St}\left(\mathbf{x} \mid \hat{\mathbf{x}}, 2\alpha, \frac{\beta}{\alpha} \mathbf{I}\right), \quad (1)$$

$$\ln \mathcal{L} \propto \ln \Gamma(\alpha + \frac{T}{2}) - \ln \Gamma(\alpha) - \frac{T}{2} \ln \beta - (\alpha + \frac{T}{2}) \ln(1 + \frac{\|\mathbf{x} - \hat{\mathbf{x}}\|_2^2}{2\beta}), \quad (2)$$

where  $\Gamma(\cdot)$  is the gamma function and  $\alpha$  and  $\beta$  are the shape and scale in the inverse gamma parameterization, which are predicted by the model along with the estimated signal  $\hat{\mathbf{x}}$ . This objective strikes a simple balance between reducing the ratio of the signal error and variance scale through the last term, while also being penalized for underestimating the variance by the second-to-last term.

**Predictive Signal-to-Noise Ratios:** Using the above probabilistic objective that directly models both signal and error magnitude allows us to construct early exit conditions expressed directly as predictive signal-to-noise ratios, providing an interpretable thresholding mechanism for early exit. The regular SNR, and SNRi (i.e., the improvement in SNR by using the estimated signal over the input mixture  $\tilde{\mathbf{x}} \in \mathbb{R}^T$ ) that can be expressed as

$$\text{SNR}(\mathbf{x}, \hat{\mathbf{x}}) = \frac{\|\mathbf{x}\|_2^2}{\|\mathbf{x} - \hat{\mathbf{x}}\|_2^2}, \quad \text{SNRi}(\mathbf{x}, \hat{\mathbf{x}}) = \frac{\text{SNR}(\mathbf{x}, \hat{\mathbf{x}})}{\text{SNR}(\mathbf{x}, \tilde{\mathbf{x}})} = \frac{\|\mathbf{x} - \tilde{\mathbf{x}}\|_2^2}{\|\mathbf{x} - \hat{\mathbf{x}}\|_2^2}. \quad (3)$$

Per our model assumptions, we have

$$\mathbf{x} \sim \mathcal{N}(\hat{\mathbf{x}}, \sigma^2 \mathbf{I}), \quad \|\mathbf{x}\|_2^2 \sim \sigma^2 \chi_T^2 \left( \frac{\|\hat{\mathbf{x}}\|_2^2}{\sigma^2} \right), \quad (4)$$

$$\|\mathbf{x} - \hat{\mathbf{x}}\|_2^2 \sim \sigma^2 \chi_T^2, \quad \|\mathbf{x} - \tilde{\mathbf{x}}\|_2^2 \sim \sigma^2 \chi_T^2 \left( \frac{\|\hat{\mathbf{x}} - \tilde{\mathbf{x}}\|_2^2}{\sigma^2} \right), \quad (5)$$

where  $\chi_T^2(\lambda)$  is a non-central chi-square distribution with non-centrality parameter  $\lambda$  and  $T$  degrees of freedom. SNRi can now be written as a ratio of (non-central) chi-square distributions,

$$\text{SNRi}(\mathbf{x}, \hat{\mathbf{x}}) = \frac{\|\mathbf{x} - \tilde{\mathbf{x}}\|_2^2}{\|\mathbf{x} - \hat{\mathbf{x}}\|_2^2} = \frac{\phi}{\epsilon}, \quad \phi \sim \sigma^2 \chi_T^2 \left( \frac{\|\hat{\mathbf{x}} - \tilde{\mathbf{x}}\|_2^2}{\sigma^2} \right), \quad \epsilon \sim \sigma^2 \chi_T^2. \quad (6)$$

These chi-square distributions are not independent, but the ratio of even dependent chi-square variables with equal degrees of freedom quickly concentrates around its mean for large  $T$ , see the appendix for details. Thus in the limit of large  $T$  we can replace the ratio with its mean and see that the expression takes the form of a shifted gamma distribution,

$$\text{SNRi}(\mathbf{x}, \hat{\mathbf{x}}) \xrightarrow{T \rightarrow \infty} 1 + \frac{\|\hat{\mathbf{x}} - \tilde{\mathbf{x}}\|_2^2}{T\sigma^2} = 1 + z, \quad z \sim \text{Gam}\left(\alpha, \frac{\|\hat{\mathbf{x}} - \tilde{\mathbf{x}}\|_2^2}{\beta T}\right). \quad (7)$$

Although simplistic, this SNR-like distribution can be used as an early-exit condition taking the error variance into account by using the gamma CDF, or by comparing quantiles of the distribution to a target SNR level.

**Decibel-scaled SNR:** SNRs are usually reported in decibels. When making use of the CDF of the SNR/SNRi distributions we can simply rescale the target SNR to non-decibel scale, but when taking the expectation of the distribution (with  $\mathbb{E}[z]$  and  $\text{Var}[z]$  denoting respectively the expected mean and variance) we use a second-order Taylor expansion,

$$\mathbb{E}[\ln(1 + z)] \approx \ln(1 + \mathbb{E}[z]) - \frac{1}{2} \frac{\text{Var}[z]}{(1 + \mathbb{E}[z])^2}. \quad (8)$$

**Mixture Model Source Separation:** When predicting multiple sources from a single mixture, the most common way to match predictions to targets is to use uPIT [39, 40]. Taking advantage of our probabilistic formulation, we instead cast this problem as a mixture model over the predicted sources such that for targets  $\mathbf{x}_s \in \mathbb{R}^T$  and estimated sources  $\hat{\mathbf{x}}_i \in \mathbb{R}^T$  the log-likelihood of each target is,

$$\ln p(\mathbf{x}_s) = \ln \sum_i^S w_i p(\mathbf{x}_s \mid \hat{\mathbf{x}}_i) = \ln \sum_i^S w_i \text{St}\left(\mathbf{x}_s \mid \hat{\mathbf{x}}_i, 2\alpha_i, \frac{\beta_i}{\alpha_i} \mathbf{I}\right), \quad (9)$$

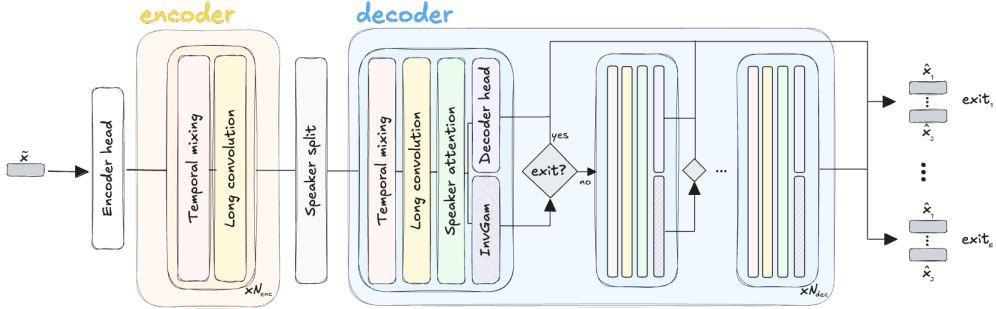


Figure 2: Detailed architecture of PRESS-Net. It consists of three parts: an encoder, an early split module and a reconstruction decoder with the ability to reconstruct early. At each exit point we estimate the expected improvement using the CDF of the parametrized gamma (modelled by the InvGam block) to determine whether we have met the exit condition or not.

where we set  $w_i = \frac{1}{S}$ . This can be stably computed in terms of per-source log-likelihoods using the LogSumExp-trick in  $\mathcal{O}(S^2)$  time on the forward pass, compared to  $\mathcal{O}(S^3)$  for uPIT using the Hungarian algorithm, and has no discontinuities.

At initialization, we found that the per-source likelihoods in Equation 9 can exhibit dramatically different scales, which causes vanishing gradient issues when one of the estimated sources are much more likely than all other sources. To remedy this, we use a scaled LogSumExp variant with temperature parameter  $\tau$  in early training and quickly anneal  $\tau$  from  $T$  to 1 with an exponential schedule during the first 0.5% of training,

$$\text{LogSumExp}_\tau(\mathbf{x}) = \tau \ln \sum_i \exp\{\tau^{-1} x_i\}, \quad \frac{d}{dx_j} \text{LogSumExp}_\tau(\mathbf{x}) = \frac{\exp\{\tau^{-1} x_j\}}{\sum_i \exp\{\tau^{-1} x_i\}}. \quad (10)$$

The temperature parameter  $\tau$  effectively controls the “sharpness” of the LogSumExp, with  $\tau > 1$  increasing gradient flow to less likely sources while recovering the regular LogSumExp at  $\tau = 1$ . This approach resembles but is distinct from other uPIT alternatives such as SinkPIT [64] and (annealed) multiple choice learning [35, 7] which also found annealing beneficial to avoid early local minima.

**Joint Early-Exit Likelihood:** When training early-exit models with permutation invariance or our mixture-likelihood, we factorize the likelihood such that all early-exits corresponding to a source are permuted as one, rather than per-exit. While advantageous from a usability perspective, this also turned out to improve the final model performance over a fully permutation-invariant approach.

### 3.2 Model Architecture

We design a time-domain audio separation network (TasNet)-family model suitable for early exit using PRESS, and denote the architecture PRESS-Net as illustrated in Figure 2. We base the initial design of the PRESS-Net architecture on building blocks from the SepReformer [47] model due to its strong performance in speech separation. Following recent trends [47, 60], we opt for an encoder-separator-decoder design where a shallow encoder/decoder pair (referred to as encoder/decoder heads in our models) down-/upsamples the audio signals whereas a separator module directly maps the encoder output to the decoder, rather than masking the encoder output as in TasNet. We do not perform any down- or upsampling in the separator network, and do not use any bias parameters anywhere in the network. We use the *Snake* [36] activation function  $\text{Snake}(x; \theta) = x + \frac{1}{\theta} \sin(\theta x)^2$  where  $\theta$  is a learnable per-channel parameter, which has previously been used to model audio data in *BigVGAN* [10] and *High-Fidelity Audio Compression with Improved RVQGAN* [27].

**Audio Encoder and Decoder Heads:** We base our encoder and decoder heads on the design from SepReformer, but instead of using strided convolutions as filterbank we employ sequence-wise patching with patch size  $P$  [19]. This filterbank design is perceptually motivated and spreads the reconstruction error evenly across both time and frequency, as also argued in *Scaling Transformers for Low-Bitrate High-Quality Speech Coding* [44]. See fig. 6 for an illustration of the blocks.

More formally, the audio encoder head processes the time-domain audio signal  $\mathbf{x} \in \mathbb{R}^T$  by passing it through a wide 1-D convolution with kernel size  $K$  which maps it to  $\mathbb{R}^T \rightarrow \mathbb{R}^{D_{enc} \times T}$ , where we

set  $D_{enc}$  to be much larger than the model dimension  $D$  to get a highly overcomplete representation before the patch operation, as argued for in ‘‘Conv-TasNet’’ [13]. The signal is then passed through an activation function and patching:  $\mathbb{R}^{D_{enc} \times T} \rightarrow \mathbb{R}^{D_{enc}P \times T/P}$ .

After the patching-based downsampling the norm of the encoded representation still depends strongly on the loudness of the input, which would cause any normalization layer (RMSNorm or other) to dramatically amplify any artifacts caused by the downsampling when the audio is quiet, which we observed to cause audible sinusoidal artifacts at the response frequency of the downsampling filter. Motivated by the findings in *Scaling Transformers for Low-Bitrate High-Quality Speech Coding* [44] and *Hyperspherical Normalization for Scalable Deep Reinforcement Learning* [29], we reduce this aliasing amplification by using ShiftNorm [29] where a non-learnable shift parameter which we set to  $c = \frac{1}{\sqrt{D_{enc}+1}}$  is concatenated to the embedding dimension, followed by an RMSNorm layer to encode the magnitude of the encoded signal in a normalized representation without excessive amplification. Finally, a linear projection maps the latent representation onto the model dimension  $D$  ( $\mathbb{R}^{(1+D_{enc})P \times T/P} \rightarrow \mathbb{R}^{D \times T/P}$ ).

The decoder head consists of a gated linear unit (GLU) layer that maps the latent representation back to  $\mathbb{R}^{D_{enc}P \times T/P}$ , followed by a wide convolution, and finally the unpatch operation. Every exit point has its own decoder head; see figs. 2 and 6.

**Separator:** We construct our separator module as a deep transformer-like stack with pre-norm, skip connections, and LayerScale [24, 55]. Specifically, for every layer  $f$  with input  $\mathbf{x}$  in the stack we compute its output as:  $\mathbf{x} \leftarrow \mathbf{x} + \boldsymbol{\alpha} f(\text{norm}(\mathbf{x}))$ , where  $\text{norm}(\cdot)$  is an RMSNorm layer with per-channel scales initialized to 1 with  $\epsilon = 10^{-2}$  as in *Scaling Transformers for Low-Bitrate High-Quality Speech Coding* [44], and  $\boldsymbol{\alpha} \in \mathbb{R}^D$  is the per-channel LayerScale scaling factors, which we initialize to  $10^{-5}$ . This allows very deep networks to be trained stably as the separator is approximately a skip connection at initialization and only later learns to integrate non-linearity as  $\boldsymbol{\alpha}$  grows.

We use the CLA (long convolution layer), GCFN (GLU-like feed-forward block with depthwise convolutions, referred to as a pointwise layer), and speaker attention layers from SepReformer, but use a linear RNN layer for long-range time-mixing in place of attention layers. These blocks are described in more detail in the appendix, and illustrated in fig. 6. We generally consider a ‘‘block’’ to be a non-pointwise layer followed by a pointwise layer, with skip connection, LayerScale and RMSNorm applied to each layer as described above.

We use *early split* as in SepReformer, where the first  $N_{\text{Enc}}$  blocks in the stack process the encoded speech mixture after which a *speaker split* module SpeakerSplit :  $\mathbb{R}^{T \times D} \rightarrow \mathbb{R}^{T \times S \times D}$  projects the refined speech mixture into  $S$  separate groups of channels, where the speaker dimension is considered a batch dimension in later processing.

After splitting, we repeat a decoder block up to  $N_{\text{Dec}}$  times which consists of (1) a linear RNN block, (2) a long convolution block and (3) a speaker attention block, see fig. 2. After each block, we may place an exit point  $E_i < N_{\text{Dec}}$  which reconstructs the current latent representation with a separate decoder head. Apart from reconstruction, each exit point parametrizes the inverse gamma distribution which we can use to evaluate whether we should exit or not. We use the same long convolution and speaker attention blocks as in SepReformer, but replace activations with Snake.

**Linear RNNs** To capture rich, long-range temporal relationships without the quadratic cost of attention [8], we use a linear RNN based on minGRU [66] and RG-LRU [25]. The recurrence  $R(\cdot, \cdot)$  takes as input  $x_t \in \mathbb{R}^D$  and  $r_t \in \mathbb{R}^D$  to produce an output sequence  $h_t \in \mathbb{R}^D$  as follows:

$$h_t = g_t \odot h_{t-1} + (1 - g_t) \odot x_t, \quad g_t = \sigma(\lambda)^{\sigma(r_t)}, \quad (11)$$

where  $\lambda$  is a learnable diagonal matrix, and  $\sigma(\cdot)$  is the sigmoid function. This parametrization ensures that  $g_t$  is bounded between 0 and 1, making the recurrence stable.  $\lambda$  is initialized such that  $\sigma(\lambda)$  is uniformly distributed between 0.9 and 0.999 as in *Griffin* [25].

Notice that  $\lambda$  being a diagonal matrix, makes the computation of  $g_t$  elementwise. Moreover, the recurrence itself operates entirely in an elementwise fashion. Since the recurrence is linear in terms of  $h_t$  and since  $g_t$  does not depend on  $h_t$ , the recurrence can be parallelized along the time dimension using a parallel associative scan [41, 38] for efficient training.

We use the quasiseparable matrix framework from ‘‘Hydra: Bidirectional State Space Models Through Generalized Matrix Mixers’’ [28], which we refer to as just Hydra bidirectionality, in order to construct

a bidirectional variant of our recurrence:

$$\text{Hydra}_R(r_t, x_t) = \text{shift}(R(r_t, x_t)) + \text{flip}(\text{shift}(R(\text{flip}(r_t), \text{flip}(x_t)))), \quad (12)$$

where  $\text{flip}(\cdot)$  reverses a sequence along the time dimension and  $\text{shift}(\cdot)$  shifts the sequence one time index to the right, discarding the final time step and prepending the sequence with a zero vector  $0 \in R^D$ . Notice that  $r_t$  and  $r_t$  are shared in both terms of the bidirectionality, such that the Hydra approach does not require additional learned parameters. This bidirectionality has been shown to give better performance than simpler alternatives like additive or concatenative approaches [28].

**Inverse Gamma Parametrization:** We model the parameters  $\alpha$  and  $\beta$  of the inverse-gamma distribution in eq. (1) with the InvGam block in fig. 6g. The block is composed of a GLU layer followed by a Snake activation, which is then linearly projected to two scalars followed by a final softplus activation to the parameters to be non-negative. To encourage the models to learn non-trivial improvement per exit-point, we further cumulatively parametrize the final  $\alpha_i$  and  $\beta_i$  for each exit point  $i$  as  $\alpha_i = \sum_j^i \tilde{\alpha}_j$ , and  $\beta_i = (\sum_j^i \tilde{\beta}_j)^{-1}$ , where  $\tilde{\alpha}_i$  and  $\tilde{\beta}_i$  are the softplus-constrained outputs from the InvGam block. This parametrization causes the inverse-gamma distributions of earlier exits to stochastically dominate later exits, such that the CDF of a given target monotonically decreases for later exits.

## 4 Experimental Setup

PRESS is evaluated on two speech separation corpora WSJ0-2mix [14], and Libri2Mix [30] and one denoising corpora, DNS2020 [63]. Descriptions of the 3 corpora can be found in appendix C.

For all datasets the models train on 4-second segments while at evaluation time the model process samples of varying length. The models train for up to 4 million steps with a batch size of 1, amounting to 4,444 hours of training data exposure.

We use the AdamW optimizer with betas of  $(0.9, 0.999)$ , and weight decay of 0.01 which we apply to only linear and convolutional layers. We use a base learning rate of  $5 \cdot 10^{-4}$ , which was found for a  $D = 64$  model with 4 exit points, and we transfer this learning rate to wider models (e.g.  $D = 128$ ) by a per-layer factor of  $\frac{D_{old}}{D_{new}}$  as described in *A Spectral Condition for Feature Learning* [4]. We use a cosine learning rate scheduler with a 5000-step linear warmup period, followed by a decay to 0.001 of the initial learning rate over the remaining training steps. During training we clip the total gradient if its L2 norm exceeds 1 when using our Student-t likelihood as loss, or 5 if using SI-SNR. All weight matrices were initialized from a normal distribution truncated at  $3\sigma$  with standard deviations set according to *A Spectral Condition for Feature Learning* [4].

We train two main model configurations: (1) PRESS-4 (S), a smaller model with model dimension  $D = 64$ ,  $P = 4$ ,  $D_{\text{Enc}} = 256$ ,  $N_{\text{Enc}} = 8$ ,  $N_{\text{Dec}} = 12$  and 4 exit points placed every 3 decoder blocks, and (2) PRESS-12 (M), a larger model with model dimension increased to  $D = 128$ ,  $N_{\text{Enc}} = 4$ ,  $N_{\text{Dec}} = 24$  and having 12 exits, placed every second decoder block.

We trained several ablation variants of PRESS-4 (S) to determine the effectiveness of (a) SI-SNR vs. Student-t log-likelihood, (b) uPIT vs. mixture-likelihood, (c) joint vs. per-exit permutation-invariance, (d) with vs. without ShiftNorm, (e) the number of exits — we train 4-, 6-, and 12-exit variants of our small model configuration with exit-points placed uniformly over depth. We evaluate all our ablations in terms of uPIT SI-SNR improvement (SI-SNRi).

We further investigate the use of the PRESS architecture on speech enhancement tasks by naively treating noise as a distinct source to be estimated, see appendix E. We generally find that this use of our architecture matches or outperforms prominent speech enhancement methods, which remained true even after 1) substituting speaker attention blocks 2) adjusting for the additional computational overhead associated with explicitly modeling the noise signal.

## 5 Results

We find that our probabilistic likelihoods in ablations (a) and (b) achieve identical performance to training with SI-SNR and uPIT. For ablation (c) we found that per-exit permutation-invariance consistently resulted in worse performance ( $-1.2$  dB for uPIT and  $-1.4$  dB for the mixture-likelihood); this

	WSJ2-Mix		Libri2Mix			GMAC/s
	SI-SNRi	SDRi	SI-SNRi	SDRi	# Params	
Conv-TasNet [13] <sup>†</sup>	15.3	15.6	12.2	12.7	5.1M	2.82
DualPathRNN [21]	18.8	19.0	16.1	16.6	2.6M	42.52
SepFormer [9]	20.4	20.5	19.2	19.4	26M	257.94
SepFormer [9] + DM <sup>†</sup>	22.3	22.5	—	—	26M	257.94
MossFormer [32] (S)	20.9	—	—	—	10.8M	— <sup>2</sup>
MossFormer [32] (M) + DM	22.5	—	—	—	25.3M	— <sup>2</sup>
MossFormer [32] (L) + DM	22.8	—	—	—	42.1M	70.4
MossFormer2 [33] + DM	24.1	—	21.7	—	55.7M	84.2
TF-GridNet [60] (S)	20.6	—	—	—	8.2M	19.2
TF-GridNet [60] (M)	22.2	—	—	—	8.4M	36.2
TF-GridNet [60] (L)	23.4	23.5	—	—	14.4M	231.1
SepMamba [49] (S) + DM	21.2	21.4	—	—	7.2M	12.46
SepMamba [49] (M) + DM	22.7	22.9	—	—	22M	37.0
SepRefomer [47] (T)	22.4	22.6	19.7	20.2	3.7M	10.4
SepRefomer [47] (S)	23.0	23.1	20.6	21.0	4.5M	21.3
SepRefomer [47] (B)	23.8	23.9	21.6	21.9	14.2M	39.8
SepRefomer [47] (M)	24.2	24.4	22.0	22.2	17.3M	81.3
SepRefomer [47] (L) + DM	25.1	25.2	—	—	55.3M	155.5
PRESS-4 @ 4 (S)	22.43	22.62	19.94	20.38	3.5M	11.1
PRESS-12 @ 4 (M)	22.68	22.93	19.75	19.71	8.5M	28.15
PRESS-12 @ 8 (M)	23.91	24.00	20.42	20.86	14.9M	52.02
PRESS-12 @ 12 (M)	24.23	24.46	20.88	21.31	21.3M	75.9

Table 1: Results on WSJ0-2Mix and Libri2Mix test sets. We evaluate our PRESS-4 (S) model on its final exit, and also show results for our larger PRESS-12 (M) model at 3 exit points. <sup>†</sup>: some values from [47].

is likely because per-exit permutation-invariance would allow the network to swap sources through the speaker attention layers, defeating much of the point of the early split architecture design. For ablation (d) we found that introducing ShiftNorm did not impact SI-SNRi performance, but did resolve the aliasing artifacts as also observed in [44]. In ablation (e) we found that increasing the number of exits from 4, 6, 12, did not worsen performance at any of the exit points, which motivated us to train larger models at the 12-exit level.

We show the performance of our models in table 1 compared with other SOTA methods, and in fig. 3 we plot performance in SI-SNRi as a function of GMAC/s, showing how PRESS models can scale their compute dynamically while remaining competitive on WSJ0-2Mix. In fig. 4 we plot calibration curves [12] for the WSJ0-2Mix training and test set, showing that while PRESS is well-calibrated in the training data there exists a significant gap between train and test conditions.

## 6 Conclusion & Future Work

We introduced the PRESS method and PRESS-Net model, achieving highly competitive speech separation performance on WSJ0-2Mix and Libri2Mix while allowing flexible compute scaling based on probabilistic early-exit conditions. Our probabilistic formulation obviated the need for conventional approaches to scale- and permutation-invariance with better usability: allowing the loudness level of audio to be predicted without loss of performance, and potentially allowing scaling the number of speakers to larger settings than uPIT. As our mixture-model approach to permutation-

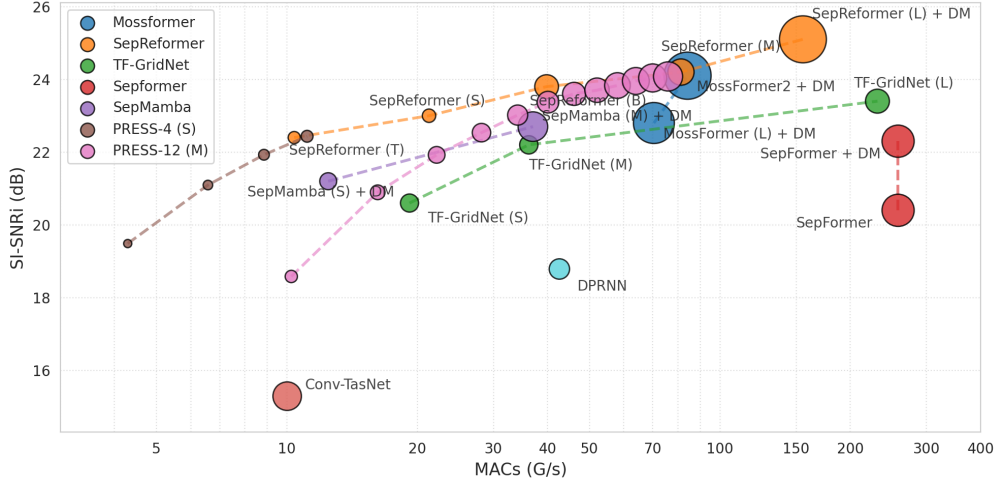
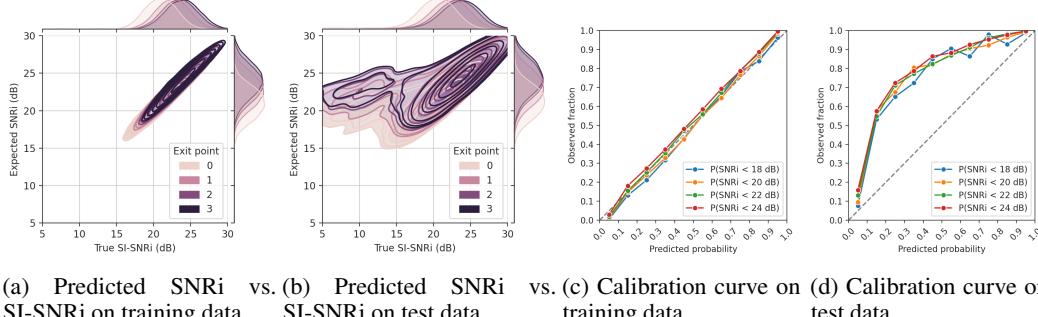


Figure 3: Performance in terms of SI-SNRi per compute (MAC/s) on the WSJ0-2mix test set, with the area of points corresponding to parameter count of models. We see that PRESS is competitive with state-of-the-art models at its later exits, but underperforms in earlier exits.



(a) Predicted SNRi vs. (b) Predicted SNRi vs. (c) Calibration curve on (d) Calibration curve on  
SI-SNRi on training data. SI-SNRi on test data. training data. test data.

Figure 4: Calibration studies of predictive SNRi distributions on WSJ0-2Mix train and test sets for our PRESS-4 (S) model. In the two left-most plots we show the density of true SI-SNRi vs. the expectation of the predicted SNRi distributions. On the right-most plots we show the proportion of observed true SI-SNRi values on the y-axis falling below the corresponding predicted CDF thresholds on the x-axis, binned in intervals of 0.1. We see that our model is well-calibrated on the training data, but there remains a large generalization gap for the WSJ0-2mix dataset.

invariance does not require the number of estimated sources and targets to match, it potentially opens the door for methods that jointly learn to model speaker presence and separation fully end-to-end.

Our predictive SNRi-like distributions proved to be very well-calibrated on training data, but showed a large generalization gap on the WSJ0-2Mix test set. This is a well known issue in deep neural networks [37]. This systematic overconfidence is not uncommon in deep neural networks [37], and importantly does invalidate the use of the uncertainty prediction in deciding the desirable exit point; however, the achieved SNRi achieved is going to be slightly less than specified due to this overconfidence. Obvious extensions to our model is to employ well-known recalibration methods to correct for the overconfidence observed e.g. using isotonic regression as suggested by [6].

One important limitation of our method which we leave for future work is early-exit across various points in time — currently we modelled a global, non-causal error variance  $\sigma^2$  per exit, but for causal, real-time applications the system must adapt to changes in environment.

Another extension of our work would be to consider iterative models, i.e. special cases of our model with a single shared block in the decoder stack repeated for each exit point. This would allow theoretically infinite scaling with compute, but if done naively couples the total parameter count to the size of the iterative block requiring more careful network design, possibly using width-scaling neural networks.

## References

- [1] Siyuan Mu and Sen Lin. *A Comprehensive Survey of Mixture-of-Experts: Algorithms, Theory, and Applications*. Apr. 18, 2025. DOI: 10.48550/arXiv.2503.07137. arXiv: 2503.07137 [cs].
- [2] Tomohiro Nakatani et al. “A Hybrid Probabilistic-Deterministic Model Recursively Enhancing Speech”. In: *ICASSP 2025 - 2025 IEEE International Conference on Acoustics, Speech and Signal Processing (ICASSP)*. Apr. 2025. DOI: 10.1109/ICASSP49660.2025.10887979.
- [3] Liang Liu et al. *A Mask Free Neural Network for Monaural Speech Enhancement*. June 2023. DOI: 10.48550/arXiv.2306.04286.
- [4] Greg Yang, James B. Simon, and Jeremy Bernstein. *A Spectral Condition for Feature Learning*. May 14, 2024. DOI: 10.48550/arXiv.2310.17813. arXiv: 2310.17813.
- [5] Fabio Montello et al. *A Survey on Dynamic Neural Networks: From Computer Vision to Multi-modal Sensor Fusion*. DOI: 10.48550/arXiv.2501.07451. arXiv: 2501.07451 [cs].
- [6] Volodymyr Kuleshov, Nathan Fenner, and Stefano Ermon. “Accurate uncertainties for deep learning using calibrated regression”. In: *35th International Conference on Machine Learning, ICML* (2018).
- [7] David Perera et al. *Annealed Multiple Choice Learning: Overcoming Limitations of Winner-takes-all with Annealing*. July 22, 2024. DOI: 10.48550/arXiv.2407.15580. arXiv: 2407.15580 [cs, eess, math, stat].
- [8] Ashish Vaswani et al. “Attention Is All You Need”. In: *Advances in Neural Information Processing Systems 30* (2017).
- [9] Cem Subakan et al. *Attention Is All You Need in Speech Separation*. arXiv, Mar. 2021. DOI: 10.48550/arXiv.2010.13154. arXiv: 2010.13154 [cs, eess].
- [10] Sang-gil Lee et al. *BigVGAN: A Universal Neural Vocoder with Large-Scale Training*. arXiv, Feb. 2023. DOI: 10.48550/arXiv.2206.04658. arXiv: 2206.04658 [cs, eess].
- [11] Surat Teerapittayanan, Bradley McDanel, and H.T. Kung. “BranchyNet: Fast inference via early exiting from deep neural networks”. In: *2016 23rd International Conference on Pattern Recognition (ICPR)*. Dec. 2016. DOI: 10.1109/ICPR.2016.7900006.
- [12] Cheng Wang. *Calibration in Deep Learning: A Survey of the State-of-the-Art*. 2024. DOI: 10.48550/arXiv.2308.01222. arXiv: 2308.01222 [cs, LG].
- [13] Yi Luo and Nima Mesgarani. “Conv-TasNet: Surpassing Ideal Time-Frequency Magnitude Masking for Speech Separation”. In: *IEEE/ACM Transactions on Audio, Speech, and Language Processing* 8 (Aug. 2019). DOI: 10.1109/TASLP.2019.2915167. arXiv: 1809.07454 [cs, eess].
- [14] John S. Garofolo, David Graff, and David Pallett. *CSR-I (WSJ0) Complete LDC93S6A*. 2007. DOI: 10.35111/ewkm-cg47.
- [15] Jens Heitkaemper et al. “Demystifying TasNet: A dissecting approach”. In: *ICASSP 2020-2020 IEEE International Conference on Acoustics, Speech and Signal Processing (ICASSP)*. IEEE. 2020.
- [16] Simone Scardapane et al. “Differentiable Branching In Deep Networks for Fast Inference”. In: *IEEE International Conference on Acoustics, Speech and Signal Processing (ICASSP)*. May 2020. DOI: 10.1109/ICASSP40776.2020.9054209.
- [17] Robin Scheibler et al. “Diffusion-based generative speech source separation”. In: *ICASSP 2023-2023 IEEE International Conference on Acoustics, Speech and Signal Processing (ICASSP)*. IEEE. 2023.
- [18] Zhifeng Kong et al. “DiffWave: A Versatile Diffusion Model for Audio Synthesis”. In: *International Conference on Learning Representations, ICLR*, 2021.
- [19] John G. Proakis and Dimitris K Manolakis. *Digital Signal Processing (4th Edition)*. 4th ed. Prentice Hall, 2006.
- [20] Sanyuan Chen et al. *Don’t Shoot Butterfly with Rifles: Multi-channel Continuous Speech Separation with Early Exit Transformer*. Oct. 23, 2020. DOI: 10.48550/arXiv.2010.12180. arXiv: 2010.12180.
- [21] Yi Luo, Zhuo Chen, and Takuya Yoshioka. *Dual-Path RNN: Efficient Long Sequence Modeling for Time-Domain Single-Channel Speech Separation*. Mar. 27, 2020. DOI: 10.48550/arXiv.1910.06379. arXiv: 1910.06379 [cs, eess].
- [22] Changlin Li et al. *Dynamic Slimmable Network*. Mar. 24, 2021. DOI: 10.48550/arXiv.2103.13258. arXiv: 2103.13258 [cs].
- [23] Mohamed Elminshawi, Srikanth Raj Chetupalli, and Emanuël A. P. Habets. “Dynamic Slimmable Network for Speech Separation”. In: *IEEE Signal Processing Letters* (2024). DOI: 10.1109/LSP.2024.3445304.
- [24] Hugo Touvron et al. “Going deeper with Image Transformers”. In: *Proceedings of the IEEE International Conference on Computer Vision* (2021). DOI: 10.1109/ICCV48922.2021.00010.
- [25] Soham De et al. *Griffin: Mixing Gated Linear Recurrences with Local Attention for Efficient Language Models*. Version 1. Feb. 29, 2024. DOI: 10.48550/arXiv.2402.19427. arXiv: 2402.19427 [cs].
- [26] Efthymios Tzinis et al. “Heterogeneous Target Speech Separation”. In: *Interspeech 2022*. Sept. 2022. DOI: 10.21437/Interspeech.2022-46. arXiv: 2204.03594 [cs, eess].

[27] Rithesh Kumar et al. *High-Fidelity Audio Compression with Improved RVQGAN*. Oct. 26, 2023. DOI: 10.48550/arXiv.2306.06546. arXiv: 2306.06546 [cs].

[28] Sukjun Hwang et al. “Hydra: Bidirectional State Space Models Through Generalized Matrix Mixers”. In: *Advances in Neural Information Processing Systems* (2024).

[29] Hojoon Lee et al. *Hyperspherical Normalization for Scalable Deep Reinforcement Learning*. Feb. 21, 2025. DOI: 10.48550/arXiv.2502.15280. arXiv: 2502.15280 [cs].

[30] Joris Cosentino et al. *LibriMix: An Open-Source Dataset for Generalizable Speech Separation*. May 22, 2020. DOI: 10.48550/arXiv.2005.11262. arXiv: 2005.11262 [eess].

[31] Anwar H Joarder. “Moments of the product and ratio of two correlated chi-square variables”. In: *Statistical Papers* 3 (2009).

[32] Shengkui Zhao and Bin Ma. *MossFormer: Pushing the Performance Limit of Monaural Speech Separation Using Gated Single-Head Transformer with Convolution-Augmented Joint Self-Attentions*. Feb. 23, 2023. DOI: 10.48550/arXiv.2302.11824. arXiv: 2302.11824 [cs].

[33] Shengkui Zhao et al. “MossFormer2: Combining Transformer and RNN-Free Recurrent Network for Enhanced Time-Domain Monaural Speech Separation”. In: *IEEE International Conference on Acoustics, Speech and Signal Processing (ICASSP)* (2024). DOI: 10.1109/ICASSP48485.2024.10445985.

[34] Ye-Xin Lu, Yang Ai, and Zhen-Hua Ling. “MP-SENet: A Speech Enhancement Model with Parallel Denoising of Magnitude and Phase Spectra”. In: Aug. 2023. DOI: 10.21437/Interspeech.2023-1441.

[35] David Perera et al. “Multiple Choice Learning for Efficient Speech Separation with Many Speakers”. In: *ICASSP IEEE International Conference on Acoustics, Speech and Signal Processing*. 2025. DOI: 10.1109/ICASSP49660.2025.10888528.

[36] Liu Ziyin, Tilman Hartwig, and Masahito Ueda. “Neural Networks Fail to Learn Periodic Functions and How to Fix It”. In: *Advances in Neural Information Processing Systems* (2020).

[37] Chuan Guo et al. “On calibration of modern neural networks”. In: *International Conference on Machine Learning (ICML)*. PMLR. 2017.

[38] Eric Martin and Chris Cundy. “Parallelizing linear recurrent neural nets over sequence length”. In: *6th International Conference on Learning Representations, ICLR* (2018).

[39] Dong Yu et al. *Permutation Invariant Training of Deep Models for Speaker-Independent Multi-talker Speech Separation*. Jan. 3, 2017. DOI: 10.48550/arXiv.1607.00325. arXiv: 1607.00325 [cs, eess].

[40] Dong Yu et al. “Permutation invariant training of deep models for speaker-independent multi-talker speech separation”. In: *IEEE International Conference on Acoustics, Speech and Signal Processing (ICASSP)* (2017). DOI: 10.1109/ICASSP.2017.7952154.

[41] Guy E Blelloch. “Prefix Sums and Their Applications”. In: () .

[42] Adam Paszke et al. “PyTorch: An imperative style, high-performance deep learning library”. In: *Advances in Neural Information Processing Systems* (2019).

[43] Riccardo Miccini et al. *Scalable Speech Enhancement with Dynamic Channel Pruning*. Dec. 22, 2024. DOI: 10.48550/arXiv.2412.17121. arXiv: 2412.17121 [eess].

[44] Julian D. Parker et al. *Scaling Transformers for Low-Bitrate High-Quality Speech Coding*. Version 1. Nov. 29, 2024. DOI: 10.48550/arXiv.2411.19842. arXiv: 2411.19842.

[45] Jonathan Le Roux et al. *SDR - Half-Baked or Well Done?* arXiv, Nov. 2018. DOI: 10.48550/arXiv.1811.02508. arXiv: 1811.02508 [cs, eess].

[46] Shahar Lutati, Eliya Nachmani, and Lior Wolf. “Separate and Diffuse: Using a Pretrained Diffusion Model for Better Source Separation”. In: *The Twelfth International Conference on Learning Representations*. 2024.

[47] Ui-Hyeop Shin et al. *Separate and Reconstruct: Asymmetric Encoder-Decoder for Speech Separation*. Oct. 11, 2024. DOI: 10.48550/arXiv.2406.05983. arXiv: 2406.05983.

[48] Shahar Lutati, Eliya Nachmani, and Lior Wolf. “SepIt: Approaching a Single Channel Speech Separation Bound”. In: *Proceedings of the Annual Conference of the International Speech Communication Association, Interspeech* (2022). DOI: 10.21437/Interspeech.2022-149.

[49] Thor Højhus Avenstrup et al. “SepMamba: State-Space Models for Speaker Separation Using Mamba”. In: *IEEE International Conference on Acoustics, Speech and Signal Processing (ICASSP)* (2025). DOI: 10.1109/ICASSP49660.2025.10888846.

[50] Mohamed Elminshawi, Srikanth Raj Chetupalli, and Emanuël A. P. Habets. “Slim-Tasnet: A Slimmable Neural Network for Speech Separation”. In: *2023 IEEE Workshop on Applications of Signal Processing to Audio and Acoustics (WASPAA)*. Oct. 2023. DOI: 10.1109/WASPAA58266.2023.10248143.

[51] Jiahui Yu et al. *Slimmable Neural Networks*. Dec. 21, 2018. DOI: 10.48550/arXiv.1812.08928. arXiv: 1812.08928 [cs].

[52] Jiahui Yu et al. “Slimmable neural networks”. In: *7th International Conference on Learning Representations (ICLR)* (2019).

[53] Edward Collin Cherry. “Some Experiments on the Recognition of Speech, with One and with Two Ears”. In: *Journal of the acoustical society of America* (1953).

[54] Shawn Tan et al. *Sparse Universal Transformer*. Oct. 11, 2023. DOI: 10.48550/arXiv.2310.07096. arXiv: 2310.07096 [cs].

[55] Mitchell Wortsman et al. “Stable and low-precision training for large-scale vision-language models”. In: *Advances in Neural Information Processing Systems* (2023).

[56] George Casella and Roger L. Berger. *Statistical inference*. 2. ed. Pacific Grove, Calif: Duxbury, 2002.

[57] Efthymios Tzinis, Zhepei Wang, and Paris Smaragdis. “Sudo Rm -Rf: Efficient Networks for Universal Audio Source Separation”. In: *30th International Workshop on Machine Learning for Signal Processing (MLSP)*. 2020. DOI: 10.1109/MLSP49062.2020.9231900.

[58] Yi Luo and Nima Mesgarani. “TaSNet: Time-Domain Audio Separation Network for Real-Time, Single-Channel Speech Separation”. In: *2018 IEEE International Conference on Acoustics, Speech and Signal Processing (ICASSP)*. Apr. 2018. DOI: 10.1109/ICASSP.2018.8462116.

[59] Zhong-Qiu Wang et al. *TF-GridNet: Integrating Full- and Sub-Band Modeling for Speech Separation*. Aug. 4, 2023. DOI: 10.48550/arXiv.2211.12433. arXiv: 2211.12433 [cs, eess].

[60] Zhong-Qiu Wang et al. *TF-GridNet: Making Time-Frequency Domain Models Great Again for Monaural Speaker Separation*. Mar. 15, 2023. DOI: 10.48550/arXiv.2209.03952. arXiv: 2209.03952 [cs, eess].

[61] Kohei Saito et al. *TF-Locoformer: Transformer with Local Modeling by Convolution for Speech Separation and Enhancement*. Aug. 2024. DOI: 10.48550/arXiv.2408.03440.

[62] Serge B Provost and Edmund M Rudiuk. “The exact density function of the ratio of two dependent linear combinations of chi-square variables”. In: *Annals of the Institute of Statistical Mathematics* (1994).

[63] Chandan KA Reddy et al. “The interspeech 2020 deep noise suppression challenge: Datasets, subjective testing framework, and challenge results”. In: *arXiv preprint arXiv:2005.13981* (2020).

[64] Hideyuki Tachibana. “Towards Listening to 10 People Simultaneously: An Efficient Permutation Invariant Training of Audio Source Separation Using Sinkhorn’s Algorithm”. In: *IEEE International Conference on Acoustics, Speech and Signal Processing (ICASSP)*. DOI: 10.1109/ICASSP39728.2021.9414508. arXiv: 2010.11871 [cs, eess].

[65] Olaf Ronneberger, Philipp Fischer, and Thomas Brox. “U-Net: Convolutional Networks for Biomedical Image Segmentation”. In: *Medical Image Computing and Computer-Assisted Intervention (MICCAI)*. Cham: Springer International Publishing, 2015.

[66] Leo Feng et al. *Were RNNs All We Needed?* Oct. 1, 2024. DOI: 10.48550/arXiv.2410.01201. arXiv: 2410.01201 [cs].

[67] Simone Scardapane et al. “Why Should We Add Early Exits to Neural Networks?” In: *Cognitive Computation 5* (Sept. 2020). DOI: 10.1007/s12559-020-09734-4. arXiv: 2004.12814 [cs, stat].

[68] Haoxu Wang and Biao Tian. *ZipEnhancer: Dual-Path Down-Up Sampling-based Zipformer for Monaural Speech Enhancement*. arXiv.org. Jan. 9, 2025.

# Appendix

## A $\chi^2$ -Ratio Approximation

In section 3.1 we claim that our model assumptions allow us to express a probabilistic SNRi in terms of the estimated error variance  $\sigma^2$ . From our likelihood we have,

$$\mathbf{x} \sim \mathcal{N}(\hat{\mathbf{x}}, \sigma^2 \mathbf{I}), \quad \sigma^2 \sim \text{InvGam}(\alpha, \beta). \quad (13)$$

which we can equivalently write as,

$$\mathbf{x} = \hat{\mathbf{x}} + \sigma \mathbf{z}, \quad \mathbf{z} \sim \mathcal{N}(\mathbf{0}, \mathbf{I}). \quad (14)$$

We then obtain

$$\phi = \|\mathbf{x} - \tilde{\mathbf{x}}\|_2^2 = \|\hat{\mathbf{x}} + \sigma \mathbf{z} - \tilde{\mathbf{x}}\|_2^2 = \sigma^2 \left\| \mathbf{z} + \frac{\hat{\mathbf{x}} - \tilde{\mathbf{x}}}{\sigma} \right\|_2^2 \sim \sigma^2 \chi_T^2 \left( \frac{\|\hat{\mathbf{x}} - \tilde{\mathbf{x}}\|_2^2}{\sigma^2} \right), \quad (15)$$

$$\epsilon = \|\mathbf{x} - \hat{\mathbf{x}}\|_2^2 = \sigma^2 \|\mathbf{z}\|_2^2 \sim \sigma^2 \chi_T^2, \quad (16)$$

$$\text{SNRi} = \frac{\phi}{\epsilon}. \quad (17)$$

Clearly, these two distributions are dependent on the same draw of  $\mathbf{z}$  and consequently the distribution of  $\frac{\phi}{\epsilon}$  does *not* take the form of a non-central F-distribution, nor can we rely on existing dependence results that assume shared sub-summations in the two associated  $\chi^2$  distributions [62] or the correlation to be known [31].

Notably, the  $\sigma^2$  scaling factors cancel in the ratio, so that the only sources of randomness are (1) the draw of  $\sigma^2$  in the non-centrality parameter of  $\phi$  and (2) the draw of  $\mathbf{z}$ . We now instead consider the limiting behavior of the ratio as  $T \rightarrow \infty$  to see how it may be approximated for large  $T$ . Since  $\|\hat{\mathbf{x}} - \tilde{\mathbf{x}}\|_2^2$  is a constant which scales linearly with  $T$ , we can rewrite the non-centrality parameter of  $\phi$  to  $T\lambda$ , where we have absorbed the constant scale into a new random variable  $\lambda = \frac{\|\hat{\mathbf{x}} - \tilde{\mathbf{x}}\|_2^2}{T\sigma^2} \sim \text{Gam}\left(\alpha, \frac{\|\hat{\mathbf{x}} - \tilde{\mathbf{x}}\|_2^2}{T\beta}\right)$ . We then have to show that for

$$\phi = X_T \sim \chi_T^2(T\lambda), \quad \epsilon = Y_T \sim \chi_T^2, \quad (18)$$

the ratio  $\frac{X_T}{Y_T}$  converges in distribution to

$$\frac{X_T}{Y_T} \xrightarrow{d} 1 + \lambda \quad \text{as} \quad T \rightarrow \infty. \quad (19)$$

We start by noting that the normalized variables  $\frac{X_T}{T}$  and  $\frac{Y_T}{T}$  have decreasing variance as  $T \rightarrow \infty$ ,

$$\mathbb{E}\left[\frac{X_T}{T} \mid \lambda\right] = \frac{\mathbb{E}[X_T \mid \lambda]}{T} = 1 + \lambda, \quad \text{Var}\left[\frac{X_T}{T} \mid \lambda\right] = \frac{\text{Var}[X_T \mid \lambda]}{T^2} = \frac{2 + 4\lambda}{T} = \mathcal{O}\left(\frac{1}{T}\right), \quad (20)$$

$$\mathbb{E}\left[\frac{Y_T}{T}\right] = \frac{\mathbb{E}[Y_T]}{T} = 1, \quad \text{Var}\left[\frac{Y_T}{T}\right] = \frac{\text{Var}[Y_T]}{T^2} = \frac{2}{T} = \mathcal{O}\left(\frac{1}{T}\right), \quad (21)$$

which implies that both normalized variables converge in probability to their expected values as  $T \rightarrow \infty$ . By Slutsky's theorem [56], the ratio  $\frac{X_T}{Y_T}$  then also converges in distribution as,

$$\frac{X_T}{Y_T} = \frac{\frac{X_T}{T}}{\frac{Y_T}{T}} \xrightarrow{d} \frac{\mathbb{E}\left[\frac{X_T}{T} \mid \lambda\right]}{\mathbb{E}\left[\frac{Y_T}{T}\right]} = 1 + \lambda \quad \text{as} \quad T \rightarrow \infty. \quad (22)$$

This convergence holds even when  $X_T$  and  $Y_T$  are not independent, as the normalized variables converge to the expected values separately.

To get a feeling for the rate of convergence, we simulate the true distribution of  $\frac{X_T}{Y_T}$  for finite  $T$  with  $\lambda \sim \text{Gam}\left(\alpha, \frac{c}{\beta}\right)$  and perform one-sample Kolmogorov-Smirnov tests comparing the empirical distribution of the ratio for 1 000 000 samples to the limiting distribution  $1 + \lambda$  in fig. 5. We set the parameters  $\alpha = 60$ ,  $\beta = 0.1$ , and  $c = 0.1$  based on the average model predictions seen during training.

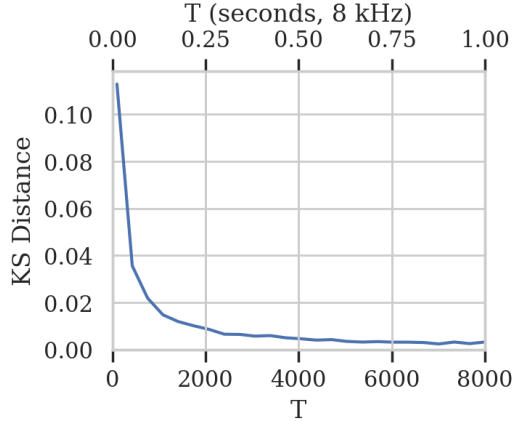


Figure 5: Kolmogorov-Smirnov (KS) test statistics for various values of  $T$ . The KS statistic represents the maximum deviation between the empirical and limiting CDFs, which is below 1% after  $T \approx 2000$ .

## B Model Architecture

Figure 6 shows additional illustrations of network blocks used in our models. Speaker attention is not shown here, but corresponds to a simple attention [8] layer with learnable linear projections  $\mathbf{P}_Q, \mathbf{P}_K, \mathbf{P}_V, \mathbf{P}_{\text{out}}$  and no positional encodings which attends over the speaker dimension as in [47], i.e., in our experiments with 2 sources the attention map is a per-timestep  $2 \times 2$  matrix.

## C Dataset Description

**WSJ0-2mix** The WSJ0-2mix [14] dataset is generated according to a Python replica<sup>1</sup> of the original Matlab implementation. 2-speaker mixtures are generated by randomly selecting utterances from different speakers in the Wall Street Journal (WSJ0) corpus. The training set contains 20,000 mixtures (30 hours), the validation set has 5,000 mixtures (8 hours), and the test set comprises 3,000 mixtures (5 hours). Speech mixtures are created by mixing pairs of utterances from different speakers at random SNRs drawn uniformly between 0 and 5 dB.

**Libri2Mix** The Libri2Mix [30] dataset is generated according to the official script<sup>2</sup>, which creates 2-speaker mixtures by randomly selecting utterances from different speakers in the LibriSpeech corpus. The loudness of each individual utterance is uniformly sampled between -25 and -33 LUFS. This mixing approach results in signal-to-noise ratios (SNRs) that follow a normal distribution with a mean of 0 dB and a standard deviation of 4.1 dB. Only the train-100set, which has 40hours/9300utterances of data, is used for training and results are reported on the test set which contains 3000 samples.

**DNS2020** The Deep Noise Suppression (DNS) Challenge 2020 [63] dataset includes two main parts: 441 hours of clean speech extracted from LibriVox audiobooks and a noise library of about 195 hours. The noise library combines 60,000 clips from AudioSet with 10,000 clips from Freesound and DEMAND databases. DNS2020 provides a mixing script but sets no guidelines for how much data should be mixed. Therefore, speech-noise mixtures were synthesized on the fly during training at SNRs between 0-20 dB. This synthesis followed the procedure provided in the original script<sup>3</sup>. Results are reported on the non-blind test set without reverberation. This test set contains 150 premixed samples.

**Sampling Rate and Downsampling** The speech separation datasets operate at 8kHz sampling rate, while DNS2020 uses a 16kHz sampling rate. This creates the only difference between our models.

<sup>1</sup><https://github.com/mpariente/pywsj0-mix>

<sup>2</sup><https://github.com/JorisCos/LibriMix>

<sup>3</sup><https://github.com/microsoft/DNS-Challenge/tree/interspeech2020/master>

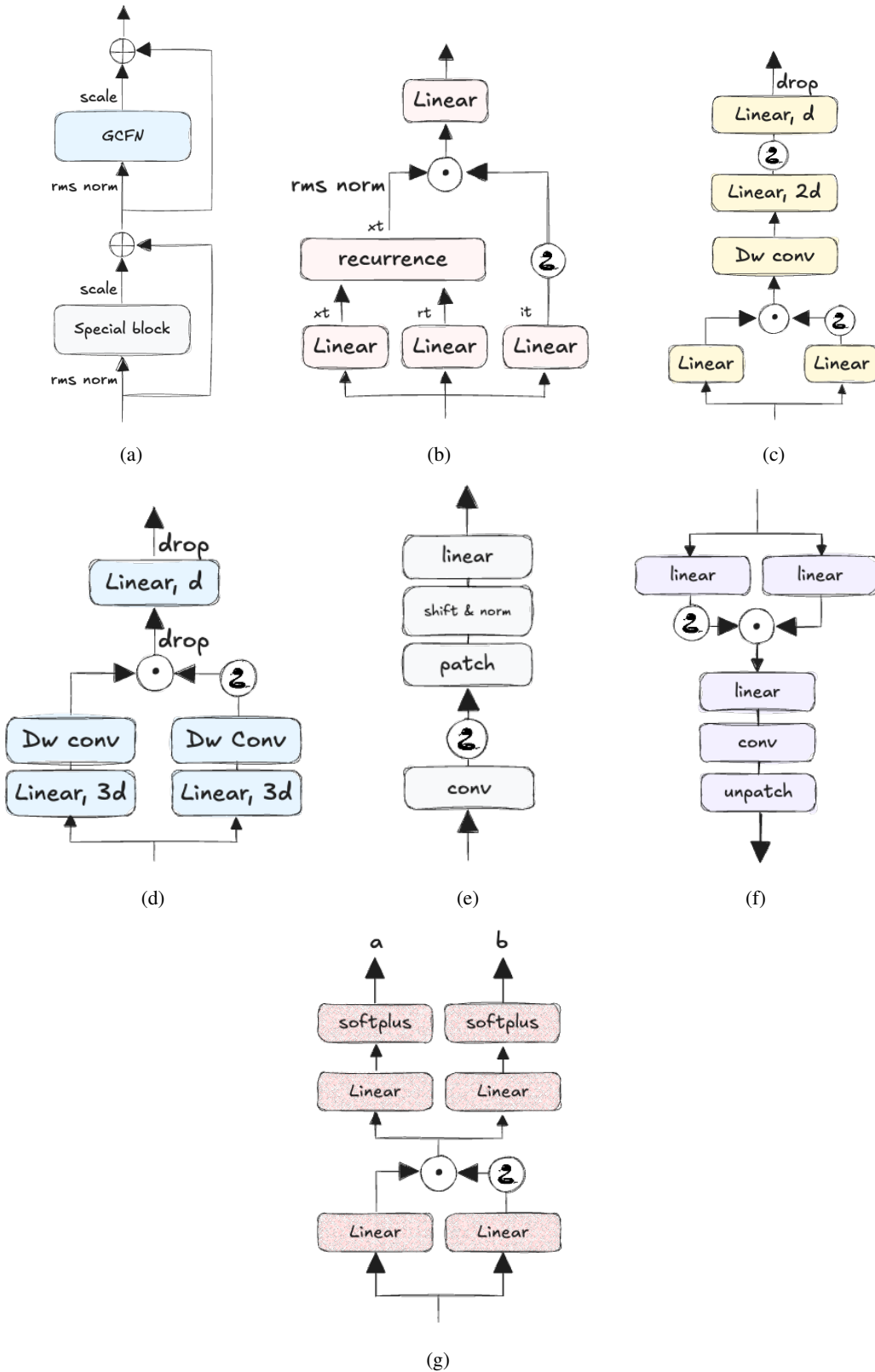


Figure 6: Detailed architecture of the blocks used. **(a)** shows the overall block architecture where the *Special block* which may be either the linear RNN **(b)**, long convolution **(c)** and speaker attention (not shown). **(d)** shows the GCFN block. **(e)** and **(f)** are the audio encoder and decoder heads respectively and **(g)** is the InvGamma parametrization block.

For 8kHz speech separation, we implement a downsampling factor of 4 in the patch encoder, while the 16kHz DNS2020 uses a factor of 8, resulting in effectively equivalent computational requirements.

## D Calibration of Predictive SNRi

As explained in Section 6 recalibration to correct for overconfidence in the predictive SNRi distributions can be achieved using isotonic regression, but since we have per-sample distributions this would require fitting a regression for every threshold of the CDF in the calibration curves. As a simple alternative, we here demonstrate that the overconfidence can also be addressed by calibrating the expected mean and variance of the associated gamma distribution by matching moments.

The mean and variance of a gamma-distributed variable  $z \sim \text{Gam}(\alpha, \beta)$  is given by

$$\mathbb{E}[z] = \alpha\beta, \quad \text{Var}[z] = \alpha\beta^2. \quad (23)$$

We construct a new gamma-distributed variable  $z' \sim \text{Gam}(\alpha', \beta')$  with mean and variance scaled by a set of two scaling parameters  $M$  and  $V$ ,

$$\mathbb{E}[z'] = M \mathbb{E}[z], \quad \text{Var}[z'] = V \text{Var}[z]. \quad (24)$$

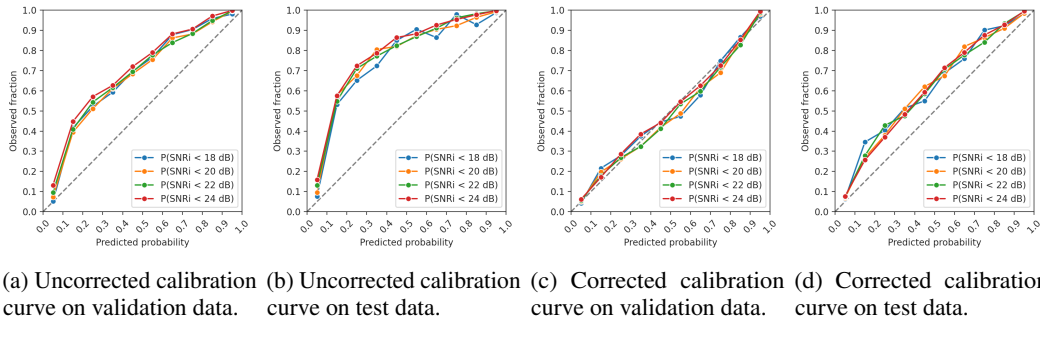
By substituting in the observed moments of the recalibration data, we find that the scaled parameters are

$$\alpha' = \frac{\mathbb{E}[z']^2}{\text{Var}[z']} = \frac{M^2}{V} \alpha, \quad \beta' = \frac{\text{Var}[z']}{\mathbb{E}[z']} = \frac{V}{M} \beta. \quad (25)$$

We can then directly minimize the expected calibration error [37] (ECE) on validation data (or generally a held-out calibration set) for the best global values of  $M$  and  $V$  to correct for any systematic shift and scale deviations. For  $C$  calibration bins, where  $N$  is the total number of samples,  $|B_c|$  is the number of samples in bin  $c$ ,  $\text{acc}(B_c)$  is the observed fraction of samples in bin  $c$ , and  $\text{conf}(B_c)$  is the predicted confidence for samples in bin  $c$  the ECE is,

$$\text{ECE} = \sum_{c=1}^C \frac{|B_c|}{N} \|\text{acc}(B_c) - \text{conf}(B_c)\|_1. \quad (26)$$

In fig. 7 we show the calibration curves on validation and test data before and after calibration on WSJ0-2mix using the validation set. The calibration curves are improved considerably, and the systematic over-estimation is corrected for. There is still over-estimation present when evaluating on the test set, but it is difficult to say if this is due to leakage between the training and validation datasets, or due to the fact that the test set contains unseen speakers, and the over-confidence is due to essentially evaluating on out-of-distribution data.



(a) Uncorrected calibration curve on validation data. (b) Uncorrected calibration curve on test data. (c) Corrected calibration curve on validation data. (d) Corrected calibration curve on test data.

Figure 7: Post-calibration results on WSJ0-2mix using fitted  $M = 0.89$  and  $V = 1.56$  learned on the validation data to correct the predicted SNRi distributions.

## E Speech Enhancement on DNS Challenge

We further evaluate our methods on the DNS 2020 dataset by treating the speech enhancement task as a source separation, where we predict both the clean speech and noise signals with our probabilistic early-exits and mixture likelihood. Surprisingly, as seen in table 2, this leads to very competitive

	SI-SDR	STOI	WB-PESQ	# Params	GMAC/s
MFNET [3]	20.32	97.98	3.43		6.09
MP-SENet [34]	21.03	98.16	3.62	2.26	40.66
TF-Locoformer [61]	<b>23.30</b>	<b>98.80</b>	<u>3.72</u>	14.97	248.62
ZipEnhancer [68]	22.22	<u>98.65</u>	<b>3.81</b>	11.34	133.48
PRESS-4 @ 4 (S)	$22.22 \pm 0.22$	98.21	3.49	3.55	11.62
PRESS-12 @ 4 (M)	$22.08 \pm 0.33$	98.45	3.48	8.57	29.06
PRESS-12 @ 8 (M)	$22.93 \pm 0.35$	98.54	3.50	14.95	53.69
PRESS-12 @ 12 (M)	$23.16 \pm 0.37$	98.49	3.45	18.14	78.32

Table 2: Performance comparison on the DNS2020 non-blind test set without reverberation, with the highest performance in **bold**, the second highest underlined, and added standard deviation on the reported mean performances.

	WSJ2-Mix		Libri2Mix	
	SI-SNRi	SDRi	SI-SNRi	SDRi
PRESS-4 @ 4 (S)	$22.43 \pm 0.06$	$22.62 \pm 0.06$	$19.94 \pm 0.06$	$20.38 \pm 0.06$
PRESS-12 @ 4 (M)	$22.68 \pm 0.05$	$22.93 \pm 0.05$	$19.75 \pm 0.05$	$19.71 \pm 0.05$
PRESS-12 @ 8 (M)	$23.91 \pm 0.05$	$24.00 \pm 0.05$	$20.42 \pm 0.05$	$20.86 \pm 0.05$
PRESS-12 @ 12 (M)	$24.23 \pm 0.05$	$24.46 \pm 0.05$	$20.88 \pm 0.05$	$21.31 \pm 0.05$

Table 3: Performance on WSJ0-2mix and Libri2Mix test sets, with added standard deviation on the reported mean performances.

performance after accounting for total GMAC/s even though our model also explicitly recovers the noise signal while other methods do not, with our smaller PRESS-4 (S) model configuration outperforming the ZipEnhancer [68] method on SI-SNRi with substantially lower compute and parameter count.

## F Training Details: Datasets, Resources and Software

We trained all models on NVIDIA GPUs with Ampere architecture or higher, using any of H100, A100, A40, A10, RTX 4090, and RTX 4070 Ti at either a university HPC cluster or commercially available GPUS with PyTorch [42] 2.7 using `torch.compile`. The PRESS-4 (S) configurations took around 2-3 days to train, while the PRESS-12 (M) configurations took around 6 days to train.

In table 3 we show the same performances as in table 1, but with added standard deviations on the reported mean performances. The results for the DNS Challenge are shown with standard deviations in table 2.

## G Scale-Invariant Student-t Likelihood

Similar to SI-SNR [45], we can construct a scale-invariant version of our likelihood by introducing a scaling parameter on the estimated signal  $\hat{x}$  which yields a modified likelihood,

$$\mathcal{L} = \text{St}\left(\mathbf{x} \mid \gamma \hat{\mathbf{x}}, 2\alpha, \frac{\beta}{\alpha}\right). \quad (27)$$

Any conjugate prior can be imposed on  $\gamma$ , but its effect would quickly be overwhelmed by the posterior for non-trivial signal length. The maximum-likelihood estimate for  $\gamma$  yields,

$$\gamma = \frac{\hat{\mathbf{x}}^\top \mathbf{x}}{\hat{\mathbf{x}}^\top \hat{\mathbf{x}}}, \quad (28)$$

which closely resembles the scale-invariance parameter in the conventional SI-SNR, but normalized by the energy in the prediction rather than the target. This scale-invariance formulation has also been used with SI-SNR to train TF-GridNet [59].

Empirical studies show that TasNets trained with log-RMS error perform comparably to those trained with SI-SDR [15]. While SI-SDR losses yield better models than RMS error, the key factor may be the logarithmic error scaling rather than scale invariance. Notably, the multivariate Student t-distribution likelihood in eq. (1) also measures errors on a log scale.

## H Limitations

In this work, we have considered the simplified case of modeling a single scalar, global variance  $\sigma^2$  of the error signal. In reality, a very non-stationary signal may also have an error signal which is not well-described by a global variance parameter, such as when one audio clip contains both a silent subsection and a noisy subsection, which renders it difficult to know when to early-exit.

Given that our predictive SNRi approximation relies on having sufficiently long sequences, this also creates a trade-off for any direct extension of our method where early-exits are decided for various block sizes, as too small blocks would give unreliable SNRi estimates.

Sequence length also directly scales the absolute value of the log-likelihood, which may accentuate the stability problems we encountered in our mixture-likelihood for very long sequences, and the LogSumExp may essentially reduce to a max operation as it did in early training in our experiments.

While we primarily evaluated our methods on clean speech separation data sets and show good performance on speech enhancement tasks, we did not investigate noisy speech separation tasks or conditions with reverberation.

## I Sample Code for Loss, Patch and ShiftNorm

We provide sample code for key parts of our normal-gamma likelihood, mixture-likelihood, patch down-/up-sampling, and ShiftNorm implemented with PyTorch [42] below.

```

1 def normal_gamma_loss(
2     preds: torch.Tensor,
3     target: torch.Tensor,
4     alpha: torch.Tensor,
5     beta: torch.Tensor,
6     per_sample: bool = False,
7 ) -> torch.Tensor:
8     T = preds.shape[-1]
9     const = (
10         torch.special.gammaln(alpha + T / 2) - torch.special.gammaln(
11             alpha)
12     ) / T - math.log(2 * math.pi) / 2
13     diff = target - preds
14     energy = torch.sum(diff**2, dim=-1) / (2 * beta)
15     coeff = alpha / T + 0.5
16     ll = const - torch.log(beta) / 2 - coeff * torch.log1p(energy)
17     return ll if per_sample else T * ll

1 from einops import rearrange
2
3 def mixture_likelihood(
4     target: torch.Tensor,
5     preds: torch.Tensor,
6     likelihood: Callable[[torch.Tensor, torch.Tensor], torch.Tensor],
7     temperature: torch.Tensor | float | None = None,
8     **kwargs,
9 ) -> torch.Tensor:
10     t = temperature if temperature is not None else 1
11     S = target.shape[1]
12     target_permuted = rearrange(target, "b s ... -> s b 1 ...")
```

```

13     ll = likelihood(target_permuted, preds, **kwargs)
14     mixture_ll = t * torch.logsumexp((ll - math.log(S)) / t, dim=2)
15     mixture_ll = rearrange(mixture_ll, "s b ... -> b s ...")
16     return mixture_ll

1   from einops import rearrange
2
3   def patch(x: torch.Tensor, P: int) -> torch.Tensor:
4       return rearrange(x, "... c (l p) -> ... (c p) l", p=P)
5
6   def unpatch(x: torch.Tensor, P: int) -> torch.Tensor:
7       return rearrange(x, "... (c p) l -> ... c (l p)", p=P)

1   class Shift(nn.Module):
2       def __init__(self, c_shift: float) -> None:
3           super().__init__()
4           self.register_buffer("c_shift", torch.full((1,), c_shift,
5                               dtype=torch.float32))
6
7       def forward(self, x: torch.Tensor) -> torch.Tensor:
8           return torch.cat((x, self.c_shift.expand(*x.shape[:-1], 1)), dim=-1)
9
10  class ShiftNorm(nn.Module):
11      def __init__(self, d_enc: int, d_model: int, c_shift: float) ->
12          None:
13          super().__init__()
14          self.shift = Shift(c_shift)
15          self.norm = RMSNorm(d_enc + 1, eps=1e-2)
16          self.proj = nn.Linear(d_enc + 1, d_model, bias=False)
17
18      def forward(self, x: torch.Tensor) -> torch.Tensor:
19          return self.proj(self.norm(self.shift(x)))

```